Research Article | Vol. 25, No. 8 | 17 Apr 2017 | OPTICS EXPRESS 8986

Optics EXPRESS

Integration of bow-tie plasmonic nano-antennas on tapered fibers

ABDUL KHALEQUE,[1,*] EVGENY G. MIRONOV,[1] JONAS H. OSÓRIO,[2] ZIYUAN LI,[3] CRISTIANO M. B. CORDEIRO,[2] LIMING LIU,[1] MARCOS A. R. FRANCO,[4] JONG-LENG LIOW,[1] AND HAROLDO T. HATTORI[1]

[1]*School of Engineering and Information Technology, The University of New South Wales (UNSW), Canberra, A.C.T., 2600 Australia*
[2]*Instituto de Física Gleb Wataghin, Unicamp, Campinas SP 13083-859, Brazil*
[3]*Department of Electronic Materials Engineering, Research School of Physics and Engineering, The Australian National University, Canberra, ACT 2601, Australia*
[4]*Divisão de Física Aplicada, Instituto de Estudos Avançados (IEAv-CTA) Trevo Cel. Av. Amarante São José dos Campos SP 12228-001, Brazil*
**abdul.khaleque@student.adfa.edu.au*

Abstract: In this article, a new and flexible approach to control the electric field enhancement of bow-tie nano-antennas by integrating them on the lateral of a tapered optical fiber is proposed. The device is driven by a Q-switched laser and the performance of a fabricated nano-antenna in a quartz slide is tested by a Surface Enhanced Raman Scattering (SERS) experiment. A refractive index sensing experiment is also performed and a sensitivity of (240 ± 30) nm/RIU is found in the 1.33-1.35 index range.

OCIS codes: (130.3120) Integrated optics devices; (240.3990) Micro-optical devices; (250.5403) Plasmonics.

References and links

1. W. L. Stutzman and G. A. Thiele, *Antenna Theory and Design* (Wiley, 2013).
2. P. Bharadwaj, B. Deutsch, and L. Novotny, "Optical antennas," Adv. Opt. Photonics **1**, 438–483 (2009).
3. T. Kosako, Y. Kadoya, and H. F. Hofmann, "Directional control of light by a nano-optical yagi–uda antenna," Nat. Photonics **4**(5), 312–315 (2010).
4. D. K. Kotter, S. D. Novack, W. D. Slafer, and P. J. Pinhero, "Theory and manufacturing processes of solar nano-antenna electromagnetic collectors," J. Sol. Energy Eng. **132**(1), 011014 (2010).
5. T. Shegai, V. D. Miljković, K. Bao, H. Xu, P. Nordlander, P. Johansson, and M. Käll, "Unidirectional broadband light emission from supported plasmonic nanowires," Nano Lett. **11**(2), 706–711 (2011).
6. R. U. Tok, C. Ow-Yang, and K. Şendur, "Unidirectional broadband radiation of honeycomb plasmonic antenna array with broken symmetry," Opt. Express **19**(23), 22731–22742 (2011).
7. N. Yu, E. Cubukcu, L. Diehl, D. Bour, S. Corzine, J. Zhu, G. Höfler, K. B. Crozier, and F. Capasso, "Bowtie plasmonic quantum cascade laser antenna," Opt. Express **15**(20), 13272–13281 (2007).
8. H. Fischer and O. J. Martin, "Engineering the optical response of plasmonic nanoantennas," Opt. Express **16**(12), 9144–9154 (2008).
9. Z. Li, H. T. Hattori, L. Fu, H. H. Tan, and C. Jagadish, "Merging photonic wire lasers and nano-antennas," J. Lightwave Technol. **29**(18), 2690–2697 (2011).
10. Z. Liu, A. Boltasseva, R. H. Pedersen, R. Bakker, A. V. Kildishev, V. P. Drachev, and V. M. Shalaev, "Plasmonic nano-antenna arrays for the visible," Metamaterials (Amst.) **2**(1), 45–51 (2008).
11. E. J. Smythe, M. D. Dickey, J. Bao, G. M. Whitesides, and F. Capasso, "Optical antenna arrays on a fiber facet for in situ surface-enhanced Raman scattering detection," Nano Lett. **9**(3), 1132–1138 (2009).
12. E. G. Mironov, Z. Li, H. T. Hattori, K. Vora, H. H. Tan, and C. Jagadish, "Titanium nano-antenna for high-power pulsed operation," J. Lightwave Technol. **31**(15), 2459–2466 (2013).
13. G. Brambilla, "Optical fibre nanowires and microwires: a review," J. Opt. **12**, 043001 (2010).
14. Fullwave, version 8.3 (RSOFT design group: 2011)
15. E. G. Mironov, Z. Li, H. T. Hattori, K. Vora, H. H. Tan, and C. Jagadish, "Titanium nano-antenna for high-power pulsed operation," J. Lightwave Technol. **31**(15), 2459–2466 (2013).
16. http://www.kemix.com/
17. L. Liu, H. T. Hattori, E. G. Mironov, and A. Khaleque, "Composite chromium and graphene oxide as saturable absorber in ytterbium-doped Q-switched fiber lasers," Appl. Opt. **53**(6), 1173–1180 (2014).
18. S. A. Maier, *Plasmonics: Fundamentals and Applications* (Springer, 2007).
19. P. C. Ashok, G. P. Singh, K. M. Tan, and K. Dholakia, "Fiber probe based microfluidic raman spectroscopy," Opt. Express **18**(8), 7642–7649 (2010).

#285107 https://doi.org/10.1364/OE.25.008986
Journal © 2017 Received 19 Jan 2017; revised 29 Mar 2017; accepted 2 Apr 2017; published 7 Apr 2017

Optics EXPRESS

20. M. V. Canamares, C. Chenal, R. L. Birke, and J. R. Lombardi, "DFT, SERS, and single-molecule SERS of crystal violet," J. Phys. Chem. C **112**(51), 20295–20300 (2008).
21. M. G. Banaee and K. B. Crozier, "Gold nanorings as substrates for surface-enhanced Raman scattering," Opt. Lett. **35**(5), 760–762 (2010).
22. W. B. Cai, B. Ren, X. Q. Li, C. X. She, F. M. Liu, X. W. Cai, and Z. Q. Tian, "Investigation of surface-enhanced Raman scattering from platinum electrodes using a confocal Raman microscope: dependence of surface roughening pretreatment," Surf. Sci. **406**(1), 9–22 (1998).
23. Z. Li, H. T. Hattori, P. Parkinson, J. Tian, L. Fu, H. H. Tan, and C. Jagadish, "A plasmonic staircase nano-antenna device with strong electric field enhancement for surface enhanced Raman scattering (SERS) applications," J. Phys. D Appl. Phys. **45**(30), 305102 (2012).
24. S. Cintra, M. E. Abdelsalam, P. N. Bartlett, J. J. Baumberg, T. A. Kelf, Y. Sugawara, and A. E. Russell, "Sculpted substrates for SERS," Faraday Discuss. **132**, 191–199 (2006).
25. S. Kedenburg, M. Vieweg, T. Gissibl, and H. Giessen, "Linear refractive index and absorption measurements of nonlinear optical liquids in the visible and near-infrared spectral region," Opt. Mater. Express **2**(11), 1588–1611 (2012).
26. E. Sani and A. Dell'Oro, "Spectral optical constants of ethanol and isopropanol from ultraviolet to far infrared," Opt. Mater. **60**, 137–141 (2016).
27. J. H. Osório, L. Mosquera, C. J. Gouveia, C. R. Biazoli, J. G. Hayashi, P. A. S. Jorge, and C. M. B. Cordeiro, "High sensitivity LPG Mach-Zehnder sensor for real-time fuel conformity analysis," Meas. Sci. Technol. **24**(1), 015102 (2013).
28. J. F. Ding, A. P. Zhang, L. Y. Shao, J. H. Yan, and S. He, "Fiber-taper seeded long-period grating pair as a highly sensitive refractive-index sensor," IEEE Photonics Technol. Lett. **17**(6), 1247–1249 (2005).
29. S. Silva, E. G. P. Pachon, M. A. R. Franco, J. G. Hayashi, F. X. Malcata, O. Frazão, P. Jorge, and C. M. B. Cordeiro, "Ultrahigh-sensitivity temperature fiber sensor based on multimode interference," Appl. Opt. **51**(16), 3236–3242 (2012).
30. F. Beltrán-Mejía, J. H. Osório, C. R. Biazoli, and C. M. B. Cordeiro, "D-microfibers," J. Lightwave Technol. **31**(16), 3056–3061 (2013).
31. J. Calderón, J. Álvarez, J. Martinez-Pastor, and D. Hill, "Polarimetric plasmonic sensing with bowtie nanoantenna arrays," Plasmonics **10**(3), 703–711 (2015).
32. H. Hu, C. Du, Q. Wang, X. Wang, and Y. Zhao, "High sensitivity internal refractive index sensor based on a photonic crystal fiber long period grating," Instrum. Sci. Technol. **45**(2), 181–189 (2017).
33. L. W. Nien, B. K. Chao, J. H. Li, and C. H. Hsueh, "Optimized sensitivity and electric field enhancement by controlling localized surface plasmon resonances for bowtie nanoring nanoantenna arrays," Plasmonics **10**(3), 553–561 (2015).
34. C. T. DeRose, R. D. Kekatpure, D. C. Trotter, A. Starbuck, J. R. Wendt, A. Yaacobi, M. R. Watts, U. Chettiar, N. Engheta, and P. S. Davids, "Electronically controlled optical beam-steering by an active phased array of metallic nanoantennas," Opt. Express **21**(4), 5198–5208 (2013).

1. Introduction

Nano-antennas are the optical equivalent of antennas [1] that are used to transmit and receive information at radio and microwave frequencies: these antennas are being used for imaging of living cells, manipulation of nano-particles, sensing and enhancement of the efficiency in solar cells [2]. Many of these applications are possible because nano-antennas can enhance photo-physical phenomena such as the local electric field [2].

In addition to dipole antennas, other antenna configurations [2] are possible such as multiple element Yagi–Uda antennas [3], spiral nano-antennas [4], plasmonic nanowire [5], honeycomb-like antenna structure [6] and bow-tie antennas [7]-such devices expand the characteristics of conventional dipole antennas as improved far-field directivity. Dipole and bow-tie antennas, on the other hand, can confine the fields in very small regions, depending on the device gap dimensions [8, 9]. An electric field enhancement factor (EF) of about 10 was achieved by Li and co-authors when the gap size was between 20 and 50 nm [9] and the wavelength of 980 nm. Besides, Liu and associates have shown a maximum electric field EF of more than 10 with the hot spot confined in a 20 nm gap (λ = 680 nm) [10]. Furthermore, a bow-tie plasmonic quantum cascade laser antenna has been reported by Yu and associates [7] where a sub-wavelength air gap between two metallic regions can enhance the electric field by more than 50 times–however, the device operated at 7.0 μm, considerably reducing the challenges of fabricating such device and its practical interest [7].

Single-element dipole or bow-tie antennas generally produce a non-directional radiation pattern: fields are localized in a small footprint to collect external light coming from a laser

Optics EXPRESS

with much larger spot-size diameter. A desirable direction is to integrate the nano-antennas with other optical components to increase their functionalities. A nano-antenna can, for example, be directly fabricated on the optical fiber tip [11]. In this setup, however, all power guided by the fiber is solely used to drive the antennas and it can also be damaged at high fluences [12]. Moreover, an array of antennas at the end of an optical fiber can reflect light back to the laser and produce instabilities in its operation.

In this article, we show, for the first time according to the best of our knowledge, the possibility to integrate the nano-antennas array on the lateral side of a tapered optical fiber. Our approach allows a flexible control of the electric field enhancement by adjusting the fiber diameter and, in consequence, the overlap between the guided field and the metallic structure. It should be noted that the optical field travelling along the fiber can, apart from driving the nano-antennas, be also used for other functions. As a demonstration of the flexibility of our method, we fabricate an array of bow-tie nano-antennas on a 9.5 μm diameter tapered fiber which is connected to a Q-switched fiber laser. The performance of the nano-antenna device is measured experimentally and the current array of nano-antennas is used as a refractive index sensor.

2. Device principle, structure and theoretical analysis

Nano-antennas enhance the incident electric field of the optical mode that travels along the taper. Light propagating in a standard optical fiber is well confined in the core, however when light reaches the micro-taper, it leaks away from the core and reaches the boundary between the air and cladding regions. The micro-taper allows light to strongly interact with the antenna. More specifically, when field is oriented along the antenna gap (*z*-direction in our case), a highly intense electric field is generated in the air gap due to the excitation of localized surface plasmons [2, 7]: a nano-antenna efficiently converts free-space propagating light into localized energy [2]. By controlling the diameter of the micro-taper, we can control the ratio of the electric field in the micro-taper with respect to the electric field at the center of a standard fiber. The net result is that, by controlling the diameter of the nano-taper, we can control the overall electric field enhancement of the combined micro-taper and nano-antenna device.

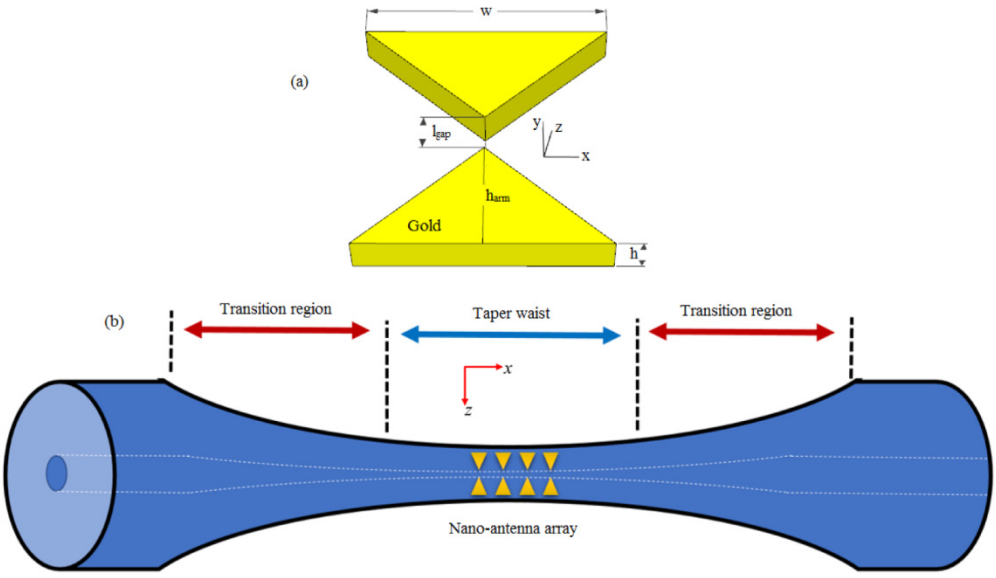

Fig. 1. Schematic diagram of (a) single bow-tie nano-antenna (b) tapered fiber including dimensions with nano-antennas array position. Fiber axis aligned with the *x*-direction, electric field is in the *z*-direction.

Optics EXPRESS

In addition, the use of micro-tapers also allow us to control the amount of energy density (fluence) that reaches the antenna, which can cause its obliteration if it is too high. In summary, we aimed to provide a flexible way to integrate nano-antennas with fiber lasers, by allowing the control of the fluence reaching the antenna and, at the same time, producing controllable gain of the combined micro-taper and nano-antenna structure.

The schematic of a single nano-antenna is shown in Fig. 1(a): the bow-tie nano-antenna is made by gold, being designed to operate around the free-space wavelength of 1090 nm and has a thickness (*h)* of 100 nm, a width (*w)* of 270 nm, a gap (l_{gap}) of 50 nm and a h_{arm} distance of *w*/2. In both simulation and experiment, the bow tie structure sits on silica. In order to create a nano-antenna array, the distance between two bow-tie nano-antennas are chosen as 2 μm and the typical position of the nano-antennas array can be seen in Fig. 1(b).

The Corning *HI 1060* singlemode optical fiber (at the designed wavelength) is used. It has a typical 125 μm cladding diameter and mode field diameter of about 6 μm in a 5.3 μm core diameter. The tapering process is based on the "flame brushing technique" [13] where an oscillating flame heats a specific region of the optical fiber reducing the glass viscosity while both fiber tips are simultaneously stretched. Pulling the fiber as it is heated causes its length to increase and, by mass conservation, its diameter to decrease [13]. The core and cladding diameters are reduced by the same ratio meaning that a 9-10 μm taper will have a sub-wavelength core diameter of 380–420 nm.

The optical properties of a single bow-tie nano-antenna is analyzed by using commercial Synopsis Fullwave [14] 3D Finite Difference Time Domain (3D FDTD) software. The structure is designed to operate with TE modes with the main electric field along the + *z* direction and directed across the gap. The computational area is terminated by perfectly matched absorbing boundary layers. The grid sizes are non-uniform and chosen as $\Delta x = \Delta z =$ 10 nm in the plane of nano-antenna with the vertical grid size of Δy = 20 nm. The grid sizes are further refined to 5 nm at the edges of the metallic layers. The time step is chosen as $\Delta t = 4.66 \times 10^{-18}$ s, which is well below the stability limit. The refractive index of silica and air are considered as 1.45 and 1.0, respectively. The material properties of gold are considered from the material library of the software [14]: the relative permittivity model of gold is modeled as,

$$\varepsilon_{gold}(\omega_{FW}) = 1 + \sum_{m=1}^{6} \frac{\Delta\varepsilon_m}{-a_m\omega_{FW}^2 - ib_m\omega_{FW} + c_m} \tag{1}$$

where a_m, b_m, c_m and $\Delta\varepsilon_m$ are coefficients that are built-in in software material library [14] and their values are shown in the *RSOFT Fullwave manual* [14]. In addition, $\omega_{FW} = 2\pi/\lambda_0$ is the *Fullwave* computational frequency where λ_0 is the free-space wavelength in μm.

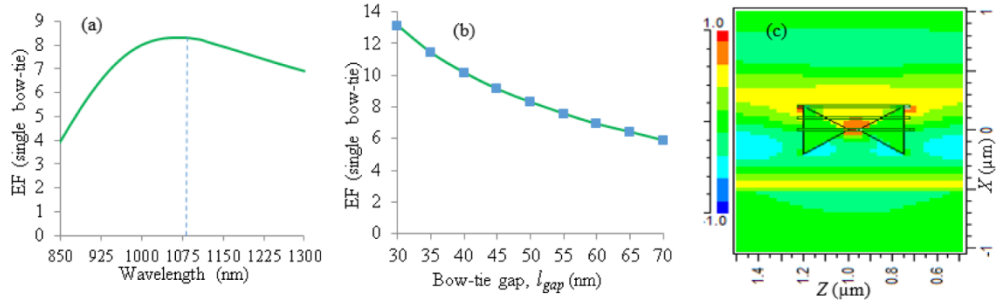

Fig. 2. Electric field enhancement factor (EF) as function of (a) wavelength (b) gap (l_{gap}) for single bow-tie nano-antenna (c) Normalized electric field (E_z) profile.

In the simulations, the light source is considered to be the main LP_{01} mode with a spot size diameter of around 6 μm. Besides, the propagation direction is assumed to be along + *x* direction. The electric field enhancement factor of a nano-antenna is defined as (EF),

Optics EXPRESS

$$EF = \frac{|E_{gap}|}{|E_{inc}|} \tag{2}$$

where $|E_{gap}|$ and $|E_{inc}|$ are the magnitude of the electric field in the middle of the nano-antenna gap and incident light to the nano-antenna respectively.

Figure 2(a) shows the electric field enhancement factor (EF) as a function of the wavelength for a single bow-tie nano-antenna with l_{gap}, h, w and h_{arm} equals 50 nm, 100 nm, 270 nm and 135 nm, respectively: it is shown that the structure resonates at 1090 nm, with a maximum electric field enhancement of EF = 8.3. In the wavelength range from 1025 nm to 1125 nm, the EF is close to 8. Moreover, the effect of changing bow-tie antenna gap dimension (l_{gap}) is shown in Fig. 2(b): the EF varies from 13 to 6.5 as the gap width increases from 30 to 70 nm. In order to see the field confinement in a bow-tie nano-antenna, the electric field (E_z) profile in the x-z plane is shown in Fig. 2(c). The electric field enhancement for TM polarization is close to 1 meaning that there is no electric field enhancement for TM modes because electric field is not oriented across the antenna gap. To be more precise, in case of TE and TM modes, the electric field is parallel (z-direction) and perpendicular (y-direction) to the metal/dielectric interface, respectively. As a result, the electric field perpendicular to the metal/dielectric interface (y-direction) is not enhanced while the electric field parallel to this interface (z-direction) is enhanced approximately 8 times.

Three dimensional (3D) simulations of an array of five bow tie nano-antennas is also studied for TE polarization in order to analyze the interaction between nano-antennas in the array. The electric field enhancement factor of 6, 5.5, 6.8, 8.4 and 11 are observed at the wavelength of 1090 nm for the 1st, 2nd, 3rd, 4th and 5th bow-tie nano-antenna in the array, respectively. The variable electric field enhancement in different antennas can be explained by the interference of the reflected optical fields from different antennas and, to a lesser extent, to coupling of light between different elements (the antennas are 2 μm apart from each other in the array, so coupling is not strong).

Although it might be possible to produce a directional array with the antennas, the array that we fabricated is small (5 antennas) and the distance between adjacent antennas (of about 2 μm) was randomly chosen. Finally, we might say that the electric field scattered through air is expected to be lower than the electric field scattered into the fiber taper region due to the higher refractive index contrast between silica and air.

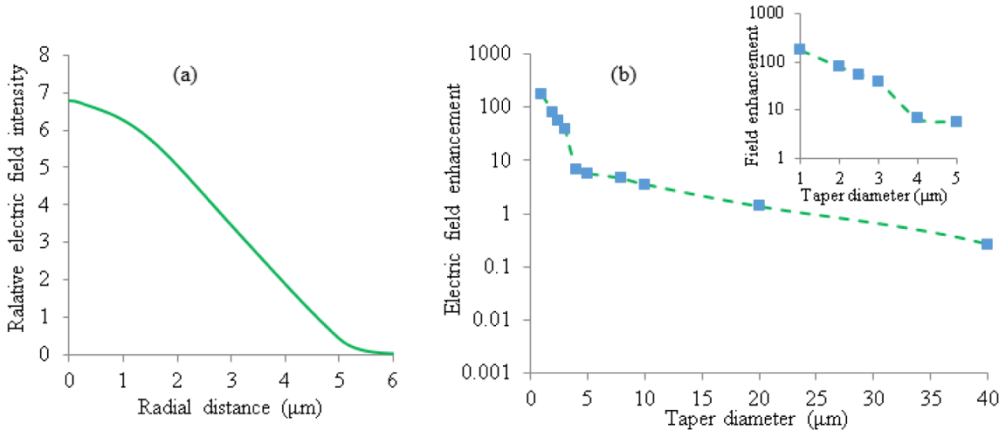

Fig. 3. (a) Relative electric field with respect to the input field intensity, in the tapered fiber (b) output electric field, as a function of radial distance of the tapered fiber.

The relative electric field intensity with respect to the input field intensity (the lunched field intensity at the taper edge is considered to be 1.0) for a tapered fiber diameter of 9.5 μm

Optics EXPRESS

as a function of the radial distance is shown in Fig. 3(a): the relative electric field is higher at the core center (radial distance = 0 μm) of the tapered fiber and then decreases gradually with the radial distance.

In order to analyze how different taper diameters affect the performance of the nano-antenna array, the electric field enhancement (logarithmic scale in the vertical axis) as a function of taper diameter is shown in Fig. 3(b). It can be observed in Fig. 3(b) that it is possible to produce a high electric field enhancement of 173 (inset) with a 1 μm diameter taper. It should be noted that it would be hard to fabricate the nano-antennas in such thin fiber and they could also be damaged by the high power–nearly all the power in the fiber leaks through the taper. An electric field enhancement of 4.02 is obtained from the nano-antenna placed on the taper with a diameter of 9.5 μm. Fabrication of nano-antennas on different diameter of the tapers provides flexibility in adjusting the fluence and the electric field enhancement in the antennas.

3. Fabrication and experimental results

Figure 4 shows the SEM image of the fabricated bow-tie antenna on the 9~10 μm optical fiber taper. In order to prepare the nanoantennas, a 100 nm thick gold layer is deposited on the tapered fiber by using Temescal BJD-2000 electron beam evaporator system. Since gold does not bind very well to silica (due to lattice constants mismatch), a 5 nm thick titanium adhesion layer is predeposited on the tapered fiber prior to gold deposition.

Bow-tie nano-antennas are fabricated on the tapered fiber by performing a milling process with a focused ion beam (FIB) (FEI Helios 600). To prepare the bow-tie geometry, gold from antenna's surrounding areas is carefully removed. As an example, five bow-tie nano-antennas are fabricated on the 9.5 μm diameter optical fiber taper in order to create the array: the distance between consecutive nano-antennas is 2 μm–a SEM image is shown in Fig. 4(a). Figure 4(b) shows the measured dimensions of a single fabricated nano-antenna: w = 265.6 nm, l_{gap} = 49.99 nm and h_{arm} = 134.3 nm. These dimensions are very close to the dimensions considered in simulations (w = 270 nm, l_{gap} = 50 nm and h_{arm} = 135 nm).

Nano-antennas are passive device which needs to be driven by a light source. Here, we are driving the nano-antennas with a Q-switched laser. It is worthy to mention that the tapered fibers with nano-antennas can be connected to different laser systems. The combination of tapered fibers with nano-antennas provides a powerful platform to integrate nano-antennas with optical fiber systems, allowing the generation of different values of electric field enhancement. Also, it allows the creation of distributed imaging and sensing systems which could be used in a plethora of applications for chemical, physical and biological analyses.

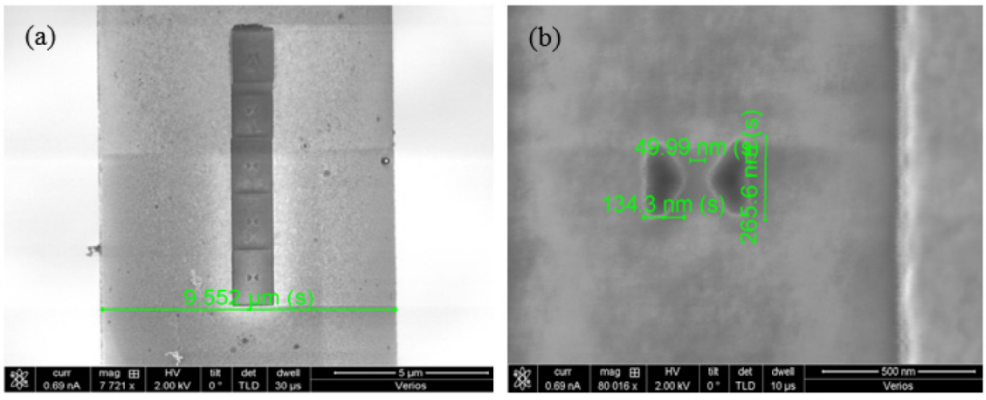

Fig. 4. Scanning Electron Microscope (SEM) image of the fabricated (a) bow-tie antenna arrays (b) single bow-tie, on the tapered optical fiber.

Optics EXPRESS

In principle, any fiber laser system working at 1090 nm could be used to drive the combined micro-taper and nano-antennas. However, in order to better control the fluence (energy per unit area) that reached the antennas, we have used a Q-switched laser. In fact, as demonstrated by Mironov and co-authors [15], a high fluence reaching the antenna can obliterate the antennas and a Q-switch laser can produce pulses with controlled fluence and, at the same time, allows the nano-antennas to cool down in the interval between consecutive pulses. In addition, the Q-switched laser has an emission spectrum broad enough to allow us to conduct the refractive index sensing measurements.

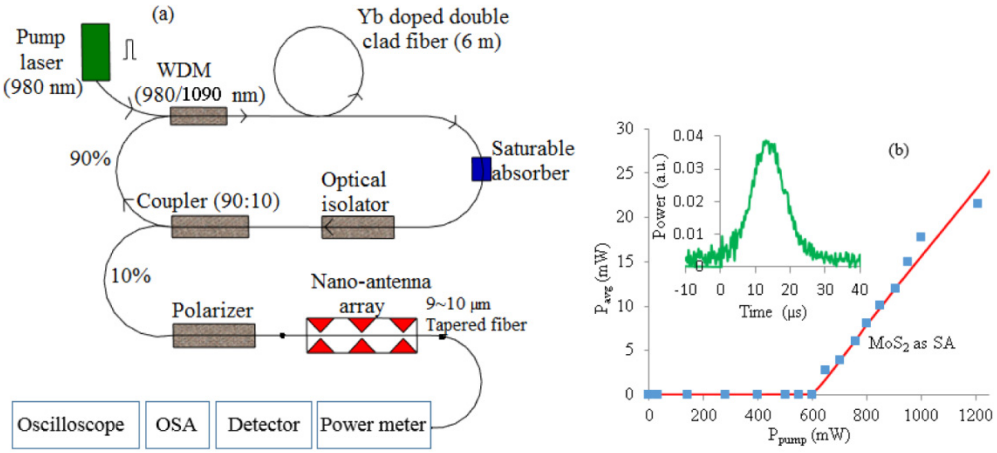

Fig. 5. Schematic of the Q-switched ring fiber laser setup (b) Average power (P_{avg}) as a function of pump power of Q-switched fiber laser while MoS_2 is used as SA (inset shows generated single pulse).

An optical pulsed fiber laser is constructed and used to drive the tapered fiber with the nano-antennas as shown in the schematic in Fig. 5(a). The fiber laser consists of a 980 nm pump laser, 6 m Yb doped fiber, MoS_2 as a saturable absorber (SA) [16, 17], an optical isolator, and a 90:10 coupler. Initially, a 980 nm continuous wave (CW) laser, which has a maximum peak power of 1.5 W and can be externally modulated at a maximum repetition rate of 3 kHz, is used to pump the ring laser as shown in Fig. 5(a). A WDM coupler is then used to couple the pump light into the ytterbium (Yb) doped (YB 1200-6/125 DC) fiber, and prevents a reflected beam at 1090 nm to return to the pump laser. After passing through 6 m of the Yb doped fiber, light passes firstly through the SA and then through the optical isolator. A small portion (10%) of the emitted light goes to a polarizing fiber and then to the fiber taper with the nano-antenna array. The fiber taper is about 15 cm long: taper waist (~5 cm) plus transition regions (~10 cm each) is then spliced with the polarizer.

Figure 5(b) shows the average output power as a function of pump power of the laser for a duty cycle of 50% (initially reducing the output power by half) and P_{pump} refers to the peak pump power while inset shows a generated single pulse for a repetition of 1 kHz: the pulse duration (FWHM) at a peak pump power of 590 mW is about 12 μs. We can reach up to around 25 mW of average power (P_{avg}) based on our constructed laser as shown in Fig. 5(b).

3.1 Measured performance of the fabricated nano-antenna

The performance of the fabricated nano-antenna is indirectly measured through a Raman experiment. Unfortunately, it was not possible to test the fabricated combined micro-taper with the nano-antennas with the existing Raman system. Firstly, the combined micro-taper with nano-antennas would not fit into the Raman setup which allowed only small samples in the system. Secondly, the whole system would need to be re-aligned and potentially damaged with the introduction of the fiber laser setup. Thirdly, the driving laser had a collimation

Optics EXPRESS

system that operated at 785 nm, meaning that the nano-antennas had to be re-designed to operate at this wavelength with a similar electric field enhancement factor. Fourthly, issues of laser safety would arise with the change of the existing driving laser since the fiber pump laser is a Class 4 laser.

Although the SERS experiment produced limited results, it allowed a comparison of the electric field enhancement of individual antennas with our calculations of electric field enhancement of the antennas. Also, the Raman signal would be lower at 1090 nm and the detectors are generally less sensitive at this wavelength. The commercial Raman system had a system of lenses which allowed the excitation of a single antenna in the fabricated antenna array in the glass slide. As described in different textbooks [18], the enhancement of the signal produced by metallic structures is proportional to the fourth power of the electric field, i.e., SERS signal $\propto|EF|^4$. In the experiment, we have used 100% ethanol with a concentration of 17 mol/l, and we have measured Raman spectra with a glass slide and glass slide with nano-antenna by using a Renishaw inVia 2 Raman spectrometer.

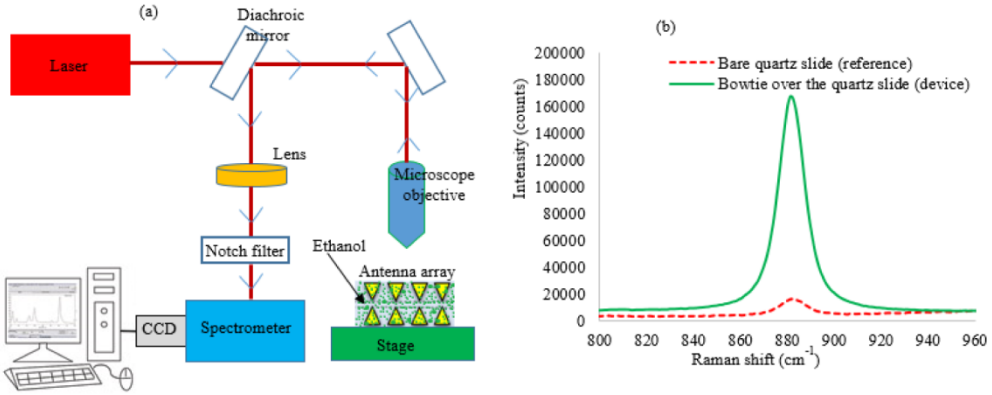

Fig. 6. (a) Schematic diagram of the Raman system for SERS measurement (b) Raman spectra of bow-tie nano-antenna fabricated on a tapered fiber and the quartz substrate used as a reference.

The schematic diagram of the Raman system for SERS measurement is shown in Fig. 6(a). The Raman spectrometer is driven by a laser source (laser in Raman system not Q-switched laser) with incident power of 13 mW with the help of dichroic mirrors and lens. The light is then focused on the sample by using another mirror and a 50x objective lens as shown in Fig. 6(a) which is only capable of illuminating one bow-tie antenna of the array due to its spot size limitation. The sample structure includes an array of five bow-tie nano-antennas on a glass plate with rescaled dimensions as l_{gap}, h, w and h_{arm} equals 50 nm, 100 nm, 170 nm and 85 nm, respectively, at the wavelength of 785 nm. An extra optical filter (notch filter) and a computer-controlled system is used to ensure the laser signal is not reaching the detector and visualize the spectrum as well as control the system, respectively. A glass plate is placed under the sample to bind the sample with ethanol solution: ethanol is dropped from top by using a pipette. We ensured that the layer of ethanol has a uniform thickness by observing the sample with a microscope. In a similar way, ethanol is placed on top of a quartz surface which is used as a reference. Figure 6(b) shows the Raman intensity of the proposed device (solid curve) compared with the quartz surface (dotted curve) under the same condition. The intensity is averaged with 25 static scans with an acquisition time of 32 seconds. The main Raman signal for ethanol [19] is present as can be seen by strong and sharp line at 880 cm^{-1} in Fig. 6(b) (solid green line).

The experimentally measured SERS EF can be calculated by [20–24]

Optics EXPRESS

$$EF_{SERS} = \frac{I_{SERS}/N_s}{I_{ref}/N_{bulk}} \tag{3}$$

where $I_{\mathrm{SERS\ and}}$ I_{ref} are the SERS intensities for the bow-tie device and from the reference quartz surface, respectively. In addition, N_{s} and N_{bulk} are the number of molecules within the excitation volume of the laser spot for the analyte in the reference region, respectively, and can be calculated as [22, 23]

$$N_s = \mu_s A_p \tag{4}$$

$$N_{bulk} = C_s N_A h A_{laser} \tag{5}$$

where μ_{s}, A_{p}, C_{s}, N_{A}, h, A_{laser} are the surface packaging density of ethanol on metal, surface area of the patterned device, concentration of the solution used for non-SERS measurement, Avogadro's number, the effective height of the focused beam, and the spot size area of the excitation laser, respectively. Table 1 shows typical values of all the parameters used in the above equations.

The above equations allow us to calculate the SERS enhancement factor for the device at the Raman shift of 880 cm^{-1} (typical Raman shift for ethanol solutions). The measured SERS EF of 4.8×10^4 is obtained for single bow-tie nano-antenna, which is higher than the theoretical *SERS EF* of 4.8×10^3 (assuming a fourth order dependence of the SERS enhancement on the local electric field enhancement EF). The measured enhancement of SERS is about ten times higher than the theoretical value because the SERS chemical factor can vary by a factor of ~10—10^2 [21, 23].

Table 1. Typical parameters [22].

Symbol	Quantity	Typical value
μ_{s}	Surface packing density of ethanol on gold	9.88×10^{18} m^{-2}
A_{p}	Surface area of the patterned device	1.44×10^{-12} m^2
C_{s}	Concentration of the solution used for non-SERS measurement	1.71×10^4 mol m^{-3}
N_{A}	Avogadro's number	6.02×10^{23} mol^{-1}
h	A parameter defined by confocal volume of the spectrometer	4.04×10^{-6} m
A_{laser}	The spot size area of the excitation laser	1.33×10^{-12} m^2

3.2 Sensing application of the proposed integrated device

The proposed integrated device can also work as a refractive index sensor. The idea is to measure the plasmonic resonance wavelength ($\Delta\lambda$) change when the external refractive index varies (Δn). The measurements are carried out with the presence of different concentration of ethanol (from 0% to 100%) in pure water. The direct transmission can be measured by an optical spectral analyzer (OSA) for different concentration of ethanol: the peak of the transmission spectrum is changed due to the change of ethanol concentration.

In terms of sensing experiment procedure, the aforementioned Q-switched fiber laser (Fig. 5(a)) is used at the wavelength of 1090 nm. The tapered fiber with fabricated nano-antennas is initially immersed in a small container with distilled water and the transmission spectrum is measured with an optical spectrum analyzer (OSA): a transmission peak is observed at the wavelength of 1096.11 nm as can be seen in inset of Fig. 7(a). Later on, a solution with an appropriate ratio of ethanol and water (e.g. 25%, 50%, 75% or 100% ethanol concentration by volume) replaces the distilled water solution and we conduct the measurement of the spectrum again. It should be mentioned that there is an interval of at least two hours between different experiments, allowing the evaporation of any residual solution left on the antennas after they are removed from the container. The resultant shift of the transmission peak ($\Delta\lambda$) for different ethanol concentration is calculated by

Optics EXPRESS

$$\Delta\lambda = \lambda_{ethanol\,(mixed)} - \lambda_{ethanol\,(100\%)} \tag{6}$$

where $\lambda_{ethanol(mixed)}$ and $\lambda_{ethanol(100\%)}$ represents the transmission peak wavelength for the ethanol concentration with mixed water and pure ethanol, respectively.

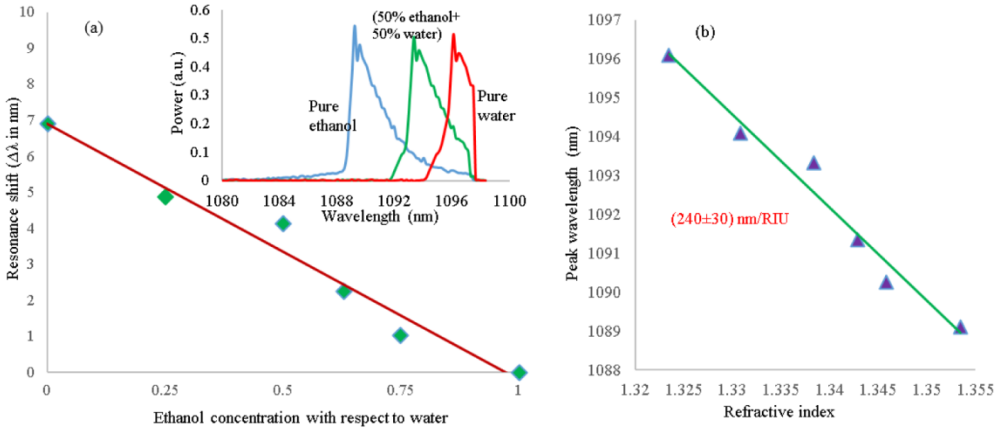

Fig. 7. (a) Resonance wavelength shift with respect to different concentration of ethanol (b) Peak wavelength as a function of corresponding refractive index of ethanol/water mixture.

The fabricated device (tapered fiber region with nano-antennas array) is immersed in different solutions and the transmission spectrum is measured as shown in inset of Fig. 7(a): the resonance peak blue shifts when the solution refractive index increases. The change in ethanol concentration leads to variations in the refractive index of ethanol solution affecting the transmission through the tapered fiber with nano-antennas array. Sellmeier equations for pure water [25] and pure ethanol [26], allows obtaining their refractive indexes at 1090 nm as 1.3235 and 1.3535, respectively. By using Eq. (7), it is possible to attain the refractive index, n, for a mixture of two liquids (pure ethanol and pure water in this case) with refractive indexes n_1 and n_2, respectively, as [27]:

$$n = \sqrt{\frac{2g+1}{1-g}} \tag{7}$$

where

$$g = \left(\frac{n_1^2-1}{n_1^2+2}\right)\phi + \left(\frac{n_2^2-1}{n_2^2+2}\right)(1-\phi) \tag{8}$$

and φ stands for the volume concentration of the liquid with refractive index of pure ethanol (n_1).

Therefore, one can replot wavelength shift data as a function of the mixture refractive index as shown in Fig. 7(b) and estimate system sensitivity as (240 ± 30) nm/RIU. The obtained value is similar to other highly sensitivity refractive index fiber sensors such as the ones based in long-period gratings interferometers [28] and multimode interference configurations [29], whose sensitivities are also around 200 nm/RIU. Other setups based on, for instance, birefringent microfibers [30] can provide higher sensitivity values. However, results found in [30] were obtained for thinner fiber tapers which needed a polishing procedure, making the system less robust.

It is true that the refractometric sensor has not produced a very high sensitivity when compared with long period gratings and interferometers. One of the reasons of a lower sensitivity is that the device was not optimized for sensing: the article reports the RI sensing

Optics EXPRESS

measurement to demonstrate an application for the nano-antenna array on the tapered fiber. Besides that, it would be possible to measure sensitivities experimentally on the magnitude order predicted by Calderón and colleagues [31] and our device is more compact compared to long periodic gratings based sensitivity devices [32]. Moreover, it would also be possible to improve the sensitivity figure by placing a circular hole within the bowtie nano-antenna triangular element as demonstrated by Nien et al. [33].

4. Conclusions

In summary, a flexible approach to integrate nano-antennas in an optical device is studied. The method is based on using tapered optical fibers to control the electric field enhancement from nano-antennas array when comparing to the electric field in the fiber core. It is shown that the amount of electric field enhancement that can be reached to the nano-antennas is ~4 and this factor can be increased up to 170 by using, for example, a 1 μm tapered fiber- the current device (tapered fiber with nano-antennas) shows the flexibility of our approach. The fabricated nano-antenna performance is measured with a Raman experiment, showing a SERS enhancement of about 4.8×10^4 for the 880 cm^{-1} line of ethanol. As an example of the application of the setup as a sensor, a refractive index probing experiment is carried on and a sensitivity value of (240 ± 30) nm/RIU is found. The integration of nano-antenna array on tapered fiber may find applications in bio-sensing, imaging, nano-particles manipulation, beam steering [34] and far-field emission collimation of semiconductor lasers.

Funding

The Asian Office of Aerospace Research and Development (AOARD US Air Force FA2386-15-1-4084); Australian Research Council (ARC LP160100253); and São Paulo Research Foundation (FAPESP) (#2014/50632-6).

Acknowledgments

The authors gratefully acknowledge the fabrication facilities provided by Australian National Fabrication Facility (ANFF ACT node, Australia). We would also acknowledge the financial support from UNSW Canberra, Australia. J. H. Osório thanks National Council for Scientific and Technological Development for financial support. The authors would thank Mr. Monir Morshed for his discussions and contributions to the revised manuscript.